HHS Public Access

Author manuscript

ACS Appl Bio Mater. Author manuscript; available in PMC 2022 February 15.

Published in final edited form as:

ACS Appl Bio Mater. 2021 February 15; 4(2): 1432–1440. doi:10.1021/acsabm.0c01324.

A Bio-Conjugated Chlorin-Based Metal–Organic Framework for Targeted Photodynamic Therapy of Triple Negative Breast and Pancreatic Cancers

Yoshie Sakamaki[#,†], **John Ozdemir**[#,†], **Zachary Heidrick**[†], **Anthony Azzun**[†], **Olivia Watson**[†], **Miu Tsuji**[†], **Christopher Salmon**[†], **Arvind Sinha**[‡], **Joseph Batta-Mpouma**[‡], **Zachary McConnell**[†], **David Fugitt**[†], **Yuchun Du**[§], **Jin-Woo Kim**[‡], **Hudson Beyzavi**[†]

[†]Department of Chemistry and Biochemistry, University of Arkansas, Fayetteville, Arkansas 72701, United States

[‡]Department of Biological and Agricultural Engineering and Institute for Nanoscience and Engineering University of Arkansas, Fayetteville, Arkansas 72701, United States

[§]Department of Biological Sciences, University of Arkansas, Fayetteville, Arkansas 72701, United States

Abstract

The field of photodynamic therapy (PDT) has continued to show promise as a potential method for treating tumors. In this work a photosensitizer (PS) has been delivered to cancer cell lines for PDT by incorporation into the metal-organic framework (MOF) as an organic linker. By functionalizing the surface of MOF nanoparticles with maltotriose the PS can efficiently target cancer cells with preferential uptake into pancreatic and breast cancer cell lines. Effective targeting overcomes some current problems with PDT including long-term photosensitivity and tumor specificity. Developing a PS with optimal absorption and stability is one of the foremost challenges in PDT and the synthesis of a chlorin which is activated by long-wavelength light and is resistant to photo-bleaching is described. This chlorin-based MOF shows anti-cancer ability several times higher than that of porphyrin-based MOFs with little toxicity to normal cell lines and no dark toxicity.

Graphical Abstract

Corresponding Author: Hudson Beyzavi, beyzavi@uark.edu; https://beyzavigroup.uark.edu.

[#]Y.S. and J.O. contributed equally to this work.

Supporting Information.

Synthesis of EDA-maltotriose, HfMOF-PFP and HfMOF-PFC, characterization of MOFs and details of in vitro experiments.

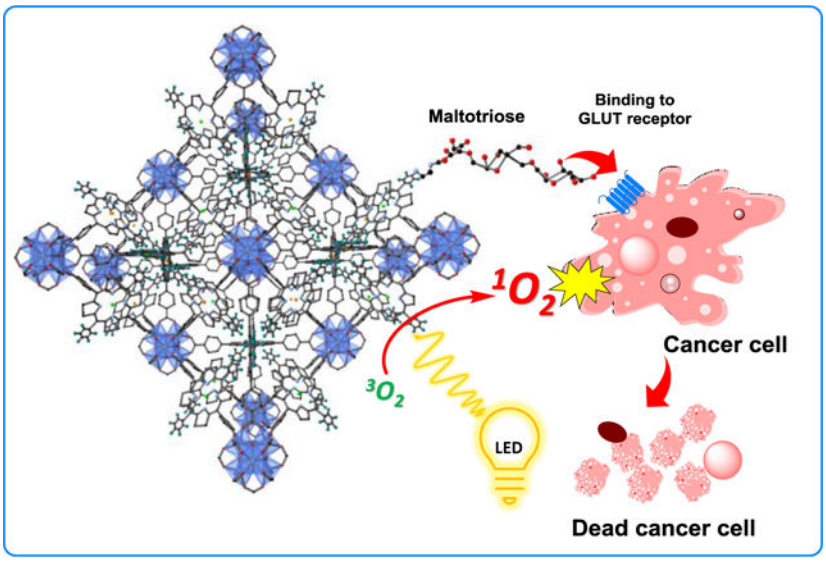

Keywords

photodynamic therapy (PDT); metal–organic framework (MOF); drug delivery system (DDS); pancreatic cancer; triple negative breast cancer (TNBC)

Introduction

Metal-organic frameworks (MOFs) have been proposed as biodegradable platforms for photodynamic therapy (PDT); in particular, research on the use of MOFs in PDT has been rapidly developing in the past five years.[1–8] PDT uses a non-toxic dye called a photosensitizer (PS) in conjunction with harmless visible or near-infrared (NIR) light to produce reactive oxygen species (ROS) in order to kill cancer cells or bacteria. PDT has the advantage of dual selectivity in that the PS can be directed to targeting cells or tissues and the light can be physically directed to the affected area.[9–11] To be viable as a PS, a compound should achieve a high quantum yield of singlet oxygen generation upon absorption in the long wavelength region (~ 800 nm). Additionally, for a PS to be a viable therapeutic, it must have preferential tumor localization, minimal dark toxicity, and simple formulation.[12] The synthesis of new PSs is of fundamental importance for developing PDT as a usable tumor treatment. Chlorin is a PS that has been clinically tested as an antitumor agent for PDT. The chlorin macrocycle is a reduced porphyrin that has a center of UV absorption blue shifted from the porphyrin absorption region. Both of these macrocycles are studied as therapeutic agents for biomedical uses.[13] Natural and synthetic chlorins are important because they have unique photophysical properties compared to the parent porphyrin, such as enhanced red light absorption and often improved fluorescence quantum yield.[13] The chlorin ring, however, can be easily converted back into porphyrin by oxidation, especially during irradiation with light as the singlet oxygen generated may oxidize the unsaturated chlorin ring.[14] Chlorin macrocycles are formed by the oxidative or reductive removal of a double bond in one of the a pyrrole rings comprising a porphyrin macrocycle.[15, 16] Stabilizing the single bond at the beta position of the pyrroles in a chlorin ring can be

achieved by installing a 5-membered pyrrolidine at this position instead of simply adding two hydrogens.[13]

Incorporating PSs into a MOF also prohibits the PS from forming molecular aggregates; this makes the crystalline MOF framework beneficial because the photophysical study of porphyrin-based macrocycles in aqueous solutions have shown that dimerization and aggregation are prevalent.[17, 18] When the PS is fixed into a supramolecular framework, as is the case in a MOF, then dimerization between the PSs cannot take place. Another issue with current PSs is the inability to discriminate between unhealthy and normal tissues, resulting in non-selective spreading of the PS throughout the body. For instance, some clinical PDT patients must avoid sunlight for at least 4 weeks after treatment.[19] Glycosylation of porphyrin and chlorin macrocycles serves to make the molecules amphiphilic,[20–22] and conjugation to sugars can also target cancer cells by the Warburg effect.[23–25]

As a continuation of our works on PDT utilizing MOFs,[1, 26] in the present work, the synthesis of a 5-ring C2 chlorin that can be incorporated into an Hf-MOF with topology similar to UiO is described. Surface glycosylation of the nano-scaled MOF crystals with maltotriose sugar gives the nanoparticles active targeting ability. The strategy of conjugation biomolecules to a MOF surface as a method to target cancer cells was explored previously by Zhou and coworkers wherein folic acid was conjugated to the surface of a porphyrinic MOF.[27] The targeting mechanism is based on binding with the glucose transporter (GLUT) receptors, which are highly expressed on cancer cell surfaces.[28–30] Maltotriose was bioconjugated to the MOF surface using a S_NAr reaction, which is the first example of such a reaction modifying a MOF surface to the best of our knowledge.

The hybrid composition of MOF frameworks allows for a multitude of functionalities to be installed onto one material. In this work, two MOF platforms have been engineered to target and kill cancer cells by the action of PDT. The two PS MOFs developed in this work, so named MA-HfMOF-PFP-Ni-Zn (MA-HfMOF-PFP) and MA-HfMOF-PFC-Ni-Zn (MA-HfMOF-PFC), were shown to be effective against three aggressive cell lines, MDA-MB-231 (triple negative breast cancer), MIA-PaCa2 (pancreatic cancer), and HeLa (cervical cancer). MDA-MB-231 represents a cancer cell line that is especially difficult to target[31] and the MIA-PaCa2 is a highly aggressive and invasive cancer cell line.[32] The cell death rates of these two cancer lines when treated with the MOF nanoparticles compared to cell death rates during analogous treatment of healthy cells demonstrates how the deliberate design of MOF nanoparticles at the compositional level can successfully enable anticancer activity.

Synthesis of EDA-MA and nano-sized MOFs

The synthesis of the chlorin linker began with preparation of 1–5-(pentafluorophenyl)dipyrromethene (**I**) (PFP-DPM)[33] which underwent condensation with methyl 4-formylbenzoate to synthesize 5,15-bis(4-carbomethoxyphenyl)-10,20-bis(pentafluorophenyl)porphyrin (**II**) (Me_2PFP; Scheme 1; Supporting Information, Section S3). After generating PFP-DPM, we modified established methods[33, 34] to produce Me_2PFP (yield: 300 mg of Me_2PFP, 18.25% yield) (Scheme 1; Supporting Information). Pure Me_2PFP was used for hydrolysis, metalation or chlorin synthesis. Metal insertion with Ni(II) of the Me_2PFP gave 5,15-bis(4-carbometholxyphenyl)-10,20-

bis(pentafluorophenyl)porphyrinato]-Ni(II) (**III**) (Ni-Me_2PFP), and then Ni-Me_2PFP underwent acidic hydrolysis of esters to give 5,15-bis(4-carboxylphenyl)-10,20 bis(pentafluorophenyl)porphyrinato]-Ni(II) (**IV**) (Ni-H_2PFP).[33,35] (Scheme 1; Supporting Information). 5,15-Bis(4-carbomethoxyphenyl)-10,20-bis(pentafluorophenyl)chlorin (**V**) (Me_2PFC) was synthesized through a 1,3-dipolar cycloaddition[13] reported previouslt by Cavaliero and coworkers.[36] (Scheme 1; Supporting Information). **V** underwent acidic hydrolysis to yield 5,15-bis(4-carboxylphenyl)-10,20-bis(pentafluorophenyl)chlorin (**VI**) (H_2PFC).

UV-vis absorption spectroscopy was used to record the absorbance of all the synthesized macrocycles (Figure 1). The H_2PFC was stored in amber vials until needed for the MOF synthesis. To compare the effectiveness of chlorin-based MOFs to that of porphyrin-based MOFs for PDT, two kinds of MOFs were prepared. For the porphyrin-based MOFs, HfMOF-PFP-Ni was synthesized by mixing a 1:1 ratio of Ni-H_2PFP and H_2PFP with $HfCl_4$ and a size-controlled synthetic methodology developed by He et al[37] resulted in nano-scale MOFs HfMOF-PFP-Ni. The chlorin-based MOFs (HfMOF-PFC-Ni) were synthesized by mixing a 1:1 ratio of Ni-H_2PFP and H_2PFC with $HfCl_4$. In order to employ the heavy atom effect that will increase the generation of reactive oxygen species,[38–40] HfMOF-PFP-Ni and HfMOF-PFC-Ni were treated with $ZnCl_2$, inserting Zn into the H_2PFP and H_2PFC ligands, respectively (Figure 2). Because Zn is a heavy atom, its presence near the PS enhances their intersystem crossing (ISC), causing an increase in $^1O_2$ production and improving their efficiency.[1, 41–44] Since it is known that the metalation of paramagnetic metal to porphyrin causes the decrease of generation of singlet oxygen,[37] we attempted to coordinate Ni^{2+} only into porphyrin but not the chlorin linkers. Ethylenediamine-maltotriose (EDA-MA) was covalently bound to the MOF surface by a S_NAr reaction between the sugar and the pentafluorobenzene substituents on the MOF linkers (Figure 2) to give MA-HfMOF-PFP and MA-HfMOF-PFC, respectively.

EDA-MA was synthesized through reaction of MA with EDA (Figure 3a). A reductive amination at the anomeric position of maltotriose was carried out according to a reported procedure.[45] The reaction progress was monitored by TLC, IR, and ^{1}H NMR. During the reaction IR spectroscopy reveals a signal at 1800 cm^{-1} which arises from the C=N bond in the imine intermediate; after the reductive amination the N–H bending vibration at 1600 cm^{-1} is found from the isolated product (Figure 3b). The signals associated with the α and β anomeric protons of the disappeared on ^{1}H NMR as the reaction proceeded (Supporting Information, Figure S6).

MOF Synthesis

The synthetic route developed by He et al[37] for the synthesis of nanoscale Zr and Hf MOFs was used in this work to synthesize two new MOFs: HfMOF-PFP and HfMOF-PFC. The Hf-MOFs used $HfCl_4$ as the metal source and were synthesized through a solvothermal reaction in DMF with acetic acid and water modulators (Supporting Information, Table S1). For HfMOF-PFP, a 1:1 ratio of H_2PFP and Ni-H_2PFP (0.165 mmol) was added to a solution of 0.33 mmol $HfCl_4$ in a solution of DMF (700 μL), acetic acid (42 μL) and water (17 μL). The same molar ratios used in the HfMOF-PFP synthesis were used in the HfMOF-PFP

synthesis but instead of porphyrin, chlorin linkers (H_2PFC and Ni-H_2PFC) were used. All MOFs were synthesized in a 15 min reaction at 120 °C; stirring was maintained at 300 rpm. After synthesis, post synthetic modification was carried out to install Zn^{2+} into coordination sites at the center of the H_2PFP linkers which was followed by the bio-conjugation step.

Bio-conjugation S_NAr reaction

Synthetic investigation began by developing model reactions to simulate the S_NAr reaction between EDA-maltotriose and a pentafluorophenyl group. First decafluorobiphenyl and EDA were selected as model molecules. Four bases were tested (diethylamine, diisopropylethyleamine, potassium *tert*-butoxide and CsF) as well as a control reaction with no base. Ultimately the reaction with no base worked the best according to ^{19}F NMR (Supporting Information, Figure S8), and it can be deduced that in this example the EDA was basic enough to undergo the reaction unaided. This result did not hold when Me_2PFP and EDA-MA were used to attempt the S_NAr reaction in DMF or DMSO. UV-vis spectroscopy was used to monitor the reaction, and it is expected that the saccharide-conjugated porphyrin displays a widening in the UV-vis absorption spectra as was observed previously.[46] Mixtures of Me_2PFP and EDA-MA were stirred in DMF for 3 hours wherein UV-Vis at the beginning and end of the reaction time showed no difference (Figure S9). When CsF was added to reaction mixture the expected widening of the absorption band was observed after 3 hours (Figure 4), which indicated a successful S_NAR reaction.

Based on the results of small-molecule reactions, surface modification of the MOF crystals was carried out with CsF as a base. In order to bioconjugate the EDA-MA, two separate solutions were prepared. One solution contained 1.5 mg CsF dissolved in 500μL of DMF while the other had 4 mg of the appropriate MOF complex mixed with 1 mg of EDA-MA in 500 μL of DMF. 100 μL of the CsF/DMF solution was pipetted into the MOF suspension. The resultant mixture was then shaken at 500 rpm for 3 hours. Then, the reaction was complete, and the resultant bio-conjugated MOF complex was rinsed with DMF and water.

Characterization of MOFs

The MOF samples were characterized using powder X-ray diffraction (pXRD), transmission electron microscopy (TEM), inductively couple plasm mass spectrometry (ICP-MS), and UV-vis. MA-HfMOF-PFP-Ni-Zn and MA-HfMOF-PFC-Ni/0Zn were characterized by TEM, zeta-potential and UV-vis. X-ray diffraction patterns of HfMOF-PFC-Ni and HfMOF-PFC-Ni-Zn were compared to calculated diffraction patterns from the single crystal structure of the MOF DBP-UiO synthesized by Lu et al.[47] Unlike DBP-UiO the HfMOF-PFC MOFs synthesized in this work do not completely match the UiO topology[48] but the HfMOF-PFC MOFs do retain structural motifs similar to UiO as evidenced by similarities in the computed and observed patterns (Figure 5a). The Ni:Zn metal ratios in the HfMOF-PFP-Ni-Zn and HfMOF-PFC-Ni-Zn samples were determined to be 1:3.1 and 1:2.7 (Table S2) using ICP-MS. This result indicates an increased incorporation of H_2PFP over Ni-H_2PFP or H_2PFC into the HfMOF-PFP-Ni and HfMOF-PFC-Ni frameworks. Comparison of particle size and morphology of the MOF particles before and after post-synthetic modification with Zn and EDA-MA using TEM can be seen in Figure 5b. This analysis reveals that the median particle

size of the nano MOFs (nMOFs) increases from the 60–70 nm range before modification to 70–80 nm after with EDA-MA conjugation (Figure S11).

This ~10 nm increase is attributed to a coating of EDA-MA around the MOF particles. Modification with EDA-MA was also analyzed by zeta potential (Table S4). Before modification with EDA-MA, the surface charge of HfMOF-PFP-Ni-Zn was measured to be is 0.651 mV (stv = 0.00146). After modification with EDA-MA, the surface of MA-HfMOF-PFP-Ni-Zn is −5.007 mV (stv = 0.00832). This slight negative shift in zeta-potential is also indicative of EDA-MA conjugating to MOFs. It is assumed that the nitrogen atoms of EDA may abstract protons from two alcohols of maltotriose resulting in a mild negative shift; moreover, this increase in negative surface charge will increase electrostatic dispersion in water. As shown in Figure 4, saccharide-conjugated porphyrin displays a widening in the UV-Vis absorption spectra. The metalation of Zn into Me_2PFC shifts the soret band from 650 nm to 630 nm (Figure 6a) as is observed in the UV-vis of the isolated Zn-Me_2-PFC (Figure 6b). The shift in the soret band when Zn is incorporated into the chlorin is also observed in MA-HfMOF-PFC-Ni-Zn when compared to HfMOF-PFC-Ni (Figure 6c).

Bioactivity Data

The selective antitumor effect of MA-HfMOF-PFC-Ni-Zn was tested *in vitro* by comparing the cell toxicity of MA-HfMOF-PFP-Ni-Zn towards three cancer cell lines: MDA-MB-231 (triple negative breast cancer) cells, MIA-PaCa2 (pancreatic cancer) cells, and HeLa (cervical cancer). MCF-10a (an immortalized human breast epithelial cell line derived from non-tumorigenic breast epithelium) was also tested. Incorporation of EDA-MA onto the MA-HfMOF-PFC-Ni-Zn particles target the GLUT receptor of cancer cells. The PDT effect of MA-HfMOF-PFP-Ni-Zn and MA-HfMOF-PFC-Ni-Zn against MDA-MB-231, MIA-PaCa2, Hela, and MCF-10a cells were measured by WST-8 assay[49] where the number of live cells is directly proportional to the amount of formazan produced. The WST-8 assay was carried out as follows: After the four cell lines were treated with MA-HfMOF-PFP-Ni-Zn and MA-HfMOF-PFC-Ni-Zn respectively, for 24 hours, the cells were washed with PBS three times and irradiated with a white LED light (100 mW/cm^2) for 30 minutes. The comparison of PDT effect for MA-HfMOF-PFP-Ni-Zn and MA-HfMOF-PFC-Ni/Z between cancer cell lines and normal cell lines is shown in Figure 7. MDA-MB-231, MIA-PaCa2, and Hela cancer cell lines were exposed to MA-HfMOF-PFP-Ni-Zn and MA-HfMOF-PFPC-Ni-Zn and irradiated with an LED light. These cancer cell lines were killed effectively after 80 μg/ml of MA-HfMOF-PFP-Ni-Zn while they were killed dramatically after 20 μg/ml of MA-HfMOF-PFC-Ni-Zn. Both MA-HfMOF-PFP-Ni-Zn and MA-HfMOF-PFC-Ni-Zn showed smaller toxicity towards the MCF-10a cell lines than cancer cell lines. To demonstrate that toxicity is dependent on irradiation with LED light, the dark toxicity of MA-HfMOF-PFP-Ni-Zn and MA-HfMOF-PFC-Ni-Zn were also tested against two cell lines used in the study, and the results are shown in Figure 7. The dark toxicity of MOFs against all three cell lines was minimal, suggesting that the toxicity of MA-HfMOF-PFP-Ni-Zn and MA-HfMOF-PFC-Ni-Zn arise only during irradiation with light. To gauge the targeting ability of the surface modified MOFs, ICP-MS was used to determine the Hf levels in the treated cells. The amount of elemental Hf in the MDA-MB-231 and MCF-10a cell lines was compared to Hf levels in the HeLa cells to determine MOFs' ability to target

cancer cells via GLUT receptor. MDA-MB-231 is also known for its highly aggressive growth, which correlates to a high expression of the GLUT receptor.[50] The result shows that cellular uptake of the maltotriose-conjugated MOFs is 20 times higher for MDA-MB-231 cells than for MCF-10a cells . This result is a strong indication that the maltotriose functionalized surface causes selective uptake of the MOFs into cancer cells. Cellular uptake of MA-HfMOF-PFC the chlorin and porphyrin such as the size, symmetry and the increased polarity of the chlorin linkers of MA-HfMOF-PFC.[44]

Conclusion

We have reported that the nano-scaled MOF MA-HfMOF-PFC-Ni-Zn can selectively target cancer cells due to maltotrionic acid conjugation on the surface of the MOF. MA-HfMOF-PFC-Ni-Zn is a well-designed drug delivery system that has been proven to actively target three cancer cell lines while showing minimal toxicity toward the normal MCF-10a cell line. The characterization of MA-HfMOF-PFC-Ni-Zn surface charge with zeta potential confirms that the dispersive effect of MOF particles can be enhanced by surface functionalization. Our previous work on this topic involved the modification of MOF nanoparticle surfaces with maltotrionic acid for similar targeted anticancer effect.[26] To determine if the MA conjugation to the surface of the MOF can achieve a cancer targeting effect within the circulation of a living sample, MA-HfMOF-PFC-Ni-Zn should be tested in a mouse model for future studies. In vivo studies by Liu's group reported that the Hf of their nMOF, Hf-TCPP-NMOF-PEG was excreted in the feces and urine of mice completely in seven days.[51] Understanding the excretion mechanism of the relevant elements will reveal to what extent toxic metal accumulation will determine therapeutic MOF dosages during in vivo experiments. Our chlorin-based nano-MOFs (MA-HfMOF-PFC-Ni-Zn) showed stronger PDT effects than porphyrin-based nano-MOFs (MA-HfMOF-PFP-Ni-Zn). Investigating and incorporating new PSs into multifunctional MOFs is a major proof of concept to make useful nanoparticles for PDT.

To date most efforts towards designing MOFs for PDT are focused on incorporating the most effective organic PS molecules within the MOF frameworks as linkers; and towards this end, more complex and efficient symmetric macrocycles should be synthesized. Inhibiting dimerization and aggregation of PSs fixed into the supramolecular crystalline frameworks means that MOFs serve as the most optimal platform for PDT. Meanwhile, functionalizing nanoparticle surfaces to increase cancer targeting[52–54] specificity will do much to broaden the viability of clinical nanomedicine. It is a much more efficient approach that must be used in future explorations of MOFs as PDT agents as it brings the PS directly to the cancer cells. Active targeting will also increase the potency of a PS so that less of the MOF needs to be administered, reducing any prolonged photosensitivity or metal toxicity. Since MA-HfMOF-PFC-Ni-Zn also contains the paramagnetic Ni^{2+} metal, it will be an excellent MRI agent.[55]

Supplementary Material

Refer to Web version on PubMed Central for supplementary material.

ACKNOWLEDGMENT

H.B. gratefully acknowledges the financial support through the startup funds from the University of Arkansas and the NIH-NIGMS (GM132906) (HB). This research has also been supported in part by Center for Advanced Surface Engineering (CASE) under the National Science Foundation (NSF) grant number OIA-1457888 and the Arkansas EPSCoR program, ASSET III (J.-W.K.).

ABBREVIATIONS

CCR2	CC chemokine receptor 2
CCL2	CC chemokine ligand 2
CCR5	CC chemokine receptor 5
TLC	thin layer chromatography

REFERENCES

1. Sakamaki Y; Ozdemir J; Heidrick Z; Watson O; Shahsavari HR; Fereidoonnezhad M; Khosropour AR; Beyzavi MH, Metal–Organic Frameworks and Covalent Organic Frameworks as Platforms for Photodynamic Therapy. Comment. Inorg. Chem 2018, 38, 238–293.
2. Song Y; Wang L; Xie Z, Metal–Organic Frameworks for Photodynamic Therapy: Emerging Synergistic Cancer Therapy. Biotechnol. J 2020, 1900382.
3. Lismont M; Dreesen L; Wuttke S, Metal-Organic Framework Nanoparticles in Photodynamic Therapy: Current Status and Perspectives. Adv. Funct. Mater 2017, 27, 1606314.
4. Lu K; He C; Lin W, A Chlorin-Based Nanoscale Metal–Organic Framework for Photodynamic Therapy of Colon Cancers. J. Am. Chem. Soc 2015, 137, 7600–7603. [PubMed: 26068094]
5. Lismont M; Dreesen L; Wuttke S, Metal-Organic Framework Nanoparticles in Photodynamic Therapy: Current Status and Perspectives. Adv. Funct. Mat 2017, 27, 1606314.
6. Lan G; Ni K; Lin W, Nanoscale Metal-Organic Frameworks for Phototherapy of Cancer. Coord. Chem. Rev 2019, 379, 65–81. [PubMed: 30739946]
7. Song Y; Wang L; Xie Z, Metal–Organic Frameworks for Photodynamic Therapy: Emerging Synergistic Cancer Therapy. Biotechnol. J 2020, 1900382.
8. Feng J; Ren W-X; Kong F; Dong Y-B, Recent Insight into Functional Crystalline Porous Frameworks for Cancer Photodynamic Therapy. Inorg. Chem. Front 2021, in press. 10.1039/D0QI01051K
9. Hammerer F; Garcia G; Chen S; Poyer F; Achelle S; Fiorini-Debuisschert C; Teulade-Fichou M-P; Maillard P, Synthesis and Characterization of Glycoconjugated Porphyrin Triphenylamine Hybrids for Targeted Two-Photon Photodynamic Therapy. J. Org. Chem 2014, 79, 1406–1417. [PubMed: 24433138]
10. Li M; Gao Y; Yuan Y; Wu Y; Song Z; Tang BZ; Liu B; Zheng QC, One-Step Formulation of Targeted Aggregation-Induced Emission Dots for Image-Guided Photodynamic Therapy of Cholangiocarcinoma. ACS Nano 2017, 11, 3922–3932. [PubMed: 28383899]
11. O'Connor AE; Gallagher WM; Byrne AT, Porphyrin and Nonporphyrin Photosensitizers in Oncology: Preclinical and Clinical Advances in Photodynamic Therapy. Photochem. Photobiol 2009, 85, 1053–74. [PubMed: 19682322]
12. Senge MO; Brandt JC, Temoporfin (Foscan®, 5,10,15,20-tetra(m-hydroxyphenyl)chlorin)–A Second-Generation Photosensitizer. Photochem. Photobiol 2011, 87, 1240–96. [PubMed: 21848905]
13. Gonzales J; Bhupathiraju NVSDK; Hart D; Yuen M; Sifuentes MP; Samarxhiu B; Maranan M; Berisha N; Batteas J; Drain CM, One-Pot Synthesis of Four Chlorin Derivatives by a Divergent Ylide. J. Org. Chem 2018, 83, 6307–6314. [PubMed: 29775305]

14. Martinez De Pinillos Bayona A; Mroz P; Thunshelle C; Hamblin MR, Design Features for Optimization of Tetrapyrrole Macrocycles as Antimicrobial and Anticancer Photosensitizers. Chem. Biol. Drug. Des 2017, 89, 192–206. [PubMed: 28205400]
15. Taniguchi M; Lindsey JS, Synthetic Chlorins, Possible Surrogates for Chlorophylls, Prepared by Derivatization of Porphyrins. Chem. Rev 2017, 117, 344–535. [PubMed: 27498781]
16. Lindsey JS, De Novo Synthesis of Gem-Dialkyl Chlorophyll Analogues for Probing and Emulating our Green World. Chem. Rev 2015, 115, 6534. [PubMed: 26068531]
17. Moreira LM; Vieira dos Santos F; Lyon JP; Maftoum-Costa M; Pacheco-Soares C; Soares da Silva N, Photodynamic Therapy: Porphyrins and Phthalocyanines as Photosensitizers. Aust. J. Chem 2008, 61, 741–754.
18. Ribó JM; Crusats J; Farrera J-A; Valero ML, Aggregation in Water Solutions of Tetrasodium Diprotonated Meso-Tetrakis(4-sulfonatophenyl)porphyrin. J. Chem. Soc., Chem. Commun 1994, 681–682.
19. Allison RR; Bagnato VS; Cuenca R; Downie GH; Sibata CH, The Future of Photodynamic Therapy in Oncology. Future Oncol. 2006, 2, 53–71. [PubMed: 16556073]
20. Fujimoto K; Miyata T; Aoyama Y, Saccharide-Directed Cell Recognition and Molecular Delivery Using Macrocyclic Saccharide Clusters: Masking of Hydrophobicity to Enhance the Saccharide Specificity. J. Am. Chem. Soc 2000, 122, 3558–3559.
21. Pasetto P; Chen X; Drain CM; Franck RW, Synthesis of Hydrolytically Stable Porphyrin C- and S-Glycoconjugates in High Yields. Chem. Commun 2001, 81–82.
22. Laville I; Pigaglio S; Blais JC; Doz F; Loock B; Maillard P; Grierson DS; Blais J, Photodynamic Efficiency of Diethylene Glycol-Linked Glycoconjugated Porphyrins in Human Retinoblastoma Cells. J. Med. Chem 2006, 49, 2558–2567. [PubMed: 16610799]
23. Singh S; Aggarwal A; Bhupathiraju NVSDK; Arianna G; Tiwari K; Drain CM, Glycosylated Porphyrins, Phthalocyanines, and Other Porphyrinoids for Diagnostics and Therapeutics. Chem. Rev 2015, 115, 10261–10306. [PubMed: 26317756]
24. Toschi A; Lee E; Thompson S; Gadir N; Yellen P; Drain CM; Ohh M; Foster DA, Phospholipase D-mTOR requirement for the Warburg effect in human cancer cells. Cancer Lett. 2010, 299, 72–79. [PubMed: 20805015]
25. Kim J.-w.; Dang CV, Cancer's Molecular Sweet Tooth and the Warburg Effect. Cancer Res. 2006, 66, 8927–8930. [PubMed: 16982728]
26. Sakamaki Y; Ozdemir J; Diaz Perez A; Heidrick Z; Watson O; Tsuji M; Salmon C; Batta-Mpouma J; Azzun A; Lomonte V; Du Y; Stenken J; Kim J-W; Beyzavi MH, Maltotriose Conjugated Metal–Organic Frameworks for Selective Targeting and Photodynamic Therapy of Triple Negative Breast Cancer Cells and Tumor Associated Macrophages. Adv. Ther 2020, 3, 2000029.
27. Park J; Jiang Q; Feng D; Mao L; Zhou H-C, Size-Controlled Synthesis of Porphyrinic Metal–Organic Framework and Functionalization for Targeted Photodynamic Therapy. J. Am. Chem. Soc 2016, 138, 3518–3525. [PubMed: 26894555]
28. Carvalho KC; Cunha IW; Rocha RM; Ayala FR; Cajaíba MM; Begnami MD; Vilela RS; Paiva GR; Andrade RG; Soares FA, GLUT1 Expression in Malignant Tumors and Its Use as an Immunodiagnostic Marker. Clinics 2011, 66, 965–972. [PubMed: 21808860]
29. Barbosa AM; Martel F, Targeting Glucose Transporters for Breast Cancer Therapy: The Effect of Natural and Synthetic Compounds. Cancers 2020, 12, 154.
30. Zhang C; Chen Z; Li W; Liu X; Tang S; Jiang L; Li M; Peng H; Lian M, Influences of Different Sugar Ligands on Targeted Delivery of Liposomes. J. Drug Target 2020, 28, 1–12. [PubMed: 31244351]
31. Han J; Lim W; You D; Jeong Y; Kim S; Lee JE; Shin TH; Lee G; Park S, Chemoresistance in the Human Triple-Negative Breast Cancer Cell Line MDA-MB-231 Induced by Doxorubicin Gradient Is Associated with Epigenetic Alterations in Histone Deacetylase. J. Oncol 2019, 2019, 1345026. [PubMed: 31275376]
32. Deer EL; González-Hernández J; Coursen JD; Shea JE; Ngatia J; Scaife CL; Firpo MA; Mulvihill SJ, Phenotype and Genotype of Pancreatic Cancer Cell Lines. Pancreas 2010, 39, 425–435. [PubMed: 20418756]

33. Moore GF; Konezny SJ; Song H.-e.; Milot RL; Blakemore JD; Lee ML; Batista VS; Schmuttenmaer CA; Crabtree RH; Brudvig GW, Bioinspired High-Potential Porphyrin Photoanodes. J. Phys. Chem 2012, 116, 4892–4902.
34. Kooriyaden FR; Sujatha S; Arunkumar C, Study of Scrambling in Porphyrin Forming Reactions: Synthesis, Structure, Photophysical, Electrochemical and Antimicrobial Studies. Polyhedron 2017, 128, 85–94.
35. Feng D; Gu Z-Y; Li J-R; Jiang H-L; Wei Z; Zhou H-C, Zirconium-Metalloporphyrin PCN-222: Mesoporous Metal–Organic Frameworks with Ultrahigh Stability as Biomimetic Catalysts. Angew. Chem. Int 2012, 51, 10307–10310.
36. Silva AMG; Tomé AC; Neves MGPMS; Silva AMS; Cavaleiro JAS, 1,3-Dipolar Cycloaddition Reactions of Porphyrins with Azomethine Ylides. J. Org. Chem 2005, 70, 2306–2314. [PubMed: 15760219]
37. He T; Xu X; Ni B; Wang H; Long Y; Hu W; Wang X, Fast and Scalable Synthesis of Uniform Zirconium-, Hafnium-Based Metal–Organic Framework Nanocrystals. Nanoscale 2017, 9, 19209–19215. [PubMed: 29188246]
38. Kim S; Ohulchanskyy TY; Bharali D; Chen Y; Pandey RK; Prasad PN, Organically Modified Silica Nanoparticles with Intraparticle Heavy-Atom Effect on the Encapsulated Photosensitizer for Enhanced Efficacy of Photodynamic Therapy. J. Phys. Chem 2009, 113, 12641–12644.
39. Gorman A; Killoran J; O'Shea C; Kenna T; Gallagher WM; O'Shea DF, In Vitro Demonstration of the Heavy-Atom Effect for Photodynamic Therapy. J. Am. Chem. Soc 2004, 126, 10619–10631. [PubMed: 15327320]
40. Zhou L; Ge X; Liu J; Zhou J; Wei S; Li F; Shen J, Internal Heavy Atom Effect of Au(III) and Pt(IV) on Hypocrellin A for Enhanced in vitro Photodynamic Therapy of Cancer. Bioorg. Med. Chem. Lett 2013, 23, 5317–24. [PubMed: 23978649]
41. Alberto ME; De Simone BC; Mazzone G; Sicilia E; Russo N, The Heavy Atom Effect on Zn(ii) Phthalocyanine Derivatives: a Theoretical Exploration of The Photophysical Properties. Phys. Chem. Chem. Phys 2015, 17, 23595–23601. [PubMed: 26299352]
42. Simone BCD; Mazzone G; Russo N; Sicilia E; Toscano M, Metal Atom Effect on the Photophysical Properties of Mg(II), Zn(II), Cd(II), and Pd(II) Tetraphenylporphyrin Complexes Proposed as Possible Drugs in Photodynamic Therapy. Molecules 2017, 22, 1093.
43. Mroz P; Bhaumik J; Dogutan DK; Aly Z; Kamal Z; Khalid L; Kee HL; Bocian DF; Holten D; Lindsey JS; Hamblin MR, Imidazole Metalloporphyrins as Photosensitizers for Photodynamic Therapy: Role of Molecular Charge, Central Metal and Hydroxyl Radical Production. Cancer Lett. 2009, 282, 63–76. [PubMed: 19346065]
44. Ezzeddine R; Al-Banaw A; Tovmasyan A; Craik JD; Batinic-Haberle I; Benov LT, Effect of Molecular Characteristics on Cellular Uptake, Subcellular Localization, and Phototoxicity of Zn(II) N-Alkylpyridylporphyrins. J Biol. Chem 2013, 288, 36579–36588. [PubMed: 24214973]
45. Basiruddin SK; Chakraborty A, One Step Synthesis of Maltose Functionalized Red Fluorescent Ag Cluster for Apecific Glycoprotein Detection and Cellular Imaging Probe. RSC Adv. 2014, 4, 43098–43104.
46. Garcia G; Hammerer F; Poyer F; Achelle S; Teulade-Fichou M-P; Maillard P, Carbohydrate-Conjugated Porphyrin Dimers: Synthesis and Photobiological Evaluation for a Potential Application in One-Photon and Two-Photon Photodynamic Therapy. Bioorg. Med. Chem 2013, 21, 153–165. [PubMed: 23218779]
47. Lu K; He C; Lin W, Nanoscale Metal–Organic Framework for Highly Effective Photodynamic Therapy of Resistant Head and Neck Cancer. J. Am. Chem. Soc 2014, 136, 16712–16715. [PubMed: 25407895]
48. Cavka JH; Jakobsen S; Olsbye U; Guillou N; Lamberti C; Bordiga S; Lillerud KP, A New Zirconium Inorganic Building Brick Forming Metal Organic Frameworks with Exceptional Stability. J. Am. Chem. Soc 2008, 130, 13850–13851. [PubMed: 18817383]
49. Tominaga H; Ishiyama M; Ohseto F; Sasamoto K; Hamamoto T; Suzuki K; Watanabe M, A Water-Soluble Tetrazolium Salt Useful for Colorimetric Cell Viability Assay. Anal Commun 1999, 36, 47–50.

50. Chen J; Lu L; Feng Y; Wang H; Dai L; Li Y; Zhang P, PKD2 Mediates Multi-Drug Resistance in Breast Cancer Cells through Modulation of P-glycoprotein Expression. Cancer Lett. 2011, 300, 48–56. [PubMed: 20934246]

51. Liu J; Yang Y; Zhu W; Yi X; Dong Z; Xu X; Chen M; Yang K; Lu G; Jiang L; Liu Z, Nanoscale Metal-Organic Frameworks for Combined Photodynamic & Radiation Therapy in Cancer Treatment. Biomaterials 2016, 97, 1–9. [PubMed: 27155362]

52. Rosenblum D; Joshi N; Tao W; Karp JM; Peer D, Progress and Challenges Towards Targeted Delivery of Cancer Therapeutics. Nat. Commun 2018, 9, 1410. [PubMed: 29650952]

53. Jiang T; Jin K; Liu X; Pang Z, 8 - Nanoparticles for Tumor Targeting. In Biopolymer-Based Composites, Jana S; Maiti S; Jana S, Eds. Woodhead Publishing: 2017; pp 221–267.

54. Gonda A; Zhao N; Shah JV; Calvelli HR; Kantamneni H; Francis NL; Ganapathy V, Engineering Tumor-Targeting Nanoparticles as Vehicles for Precision Nanomedicine. Med One 2019, 4, e190021. [PubMed: 31592196]

55. Dommaschk M; Peters M; Gutzeit F; Schütt C; Näther C; Sönnichsen FD; Tiwari S; Riedel C; Boretius S; Herges R, Photoswitchable Magnetic Resonance Imaging Contrast by Improved Light-Driven Coordination-Induced Spin State Switch. J. Am. Chem. Soc 2015, 137, 7552–7555. [PubMed: 25914182]

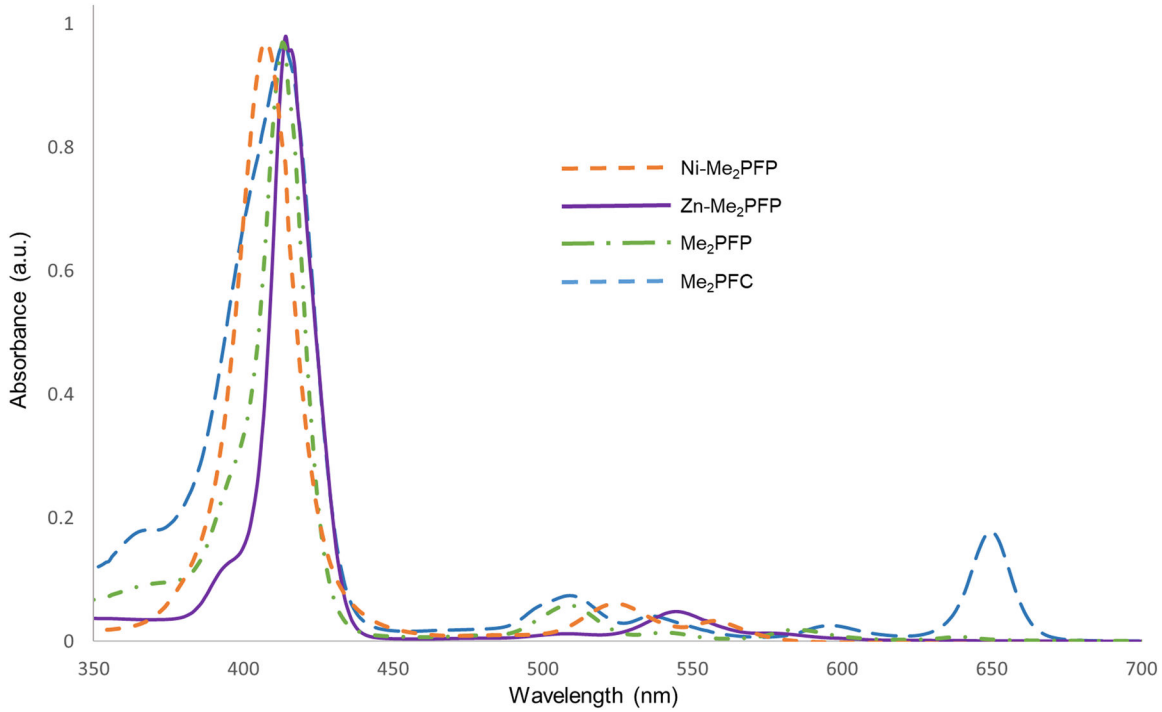

Figure 1.
UV-vis spectra of Me_2PFC, Zn-Me_2PFP, Me_2PFP, and Ni-Me_2PFP.

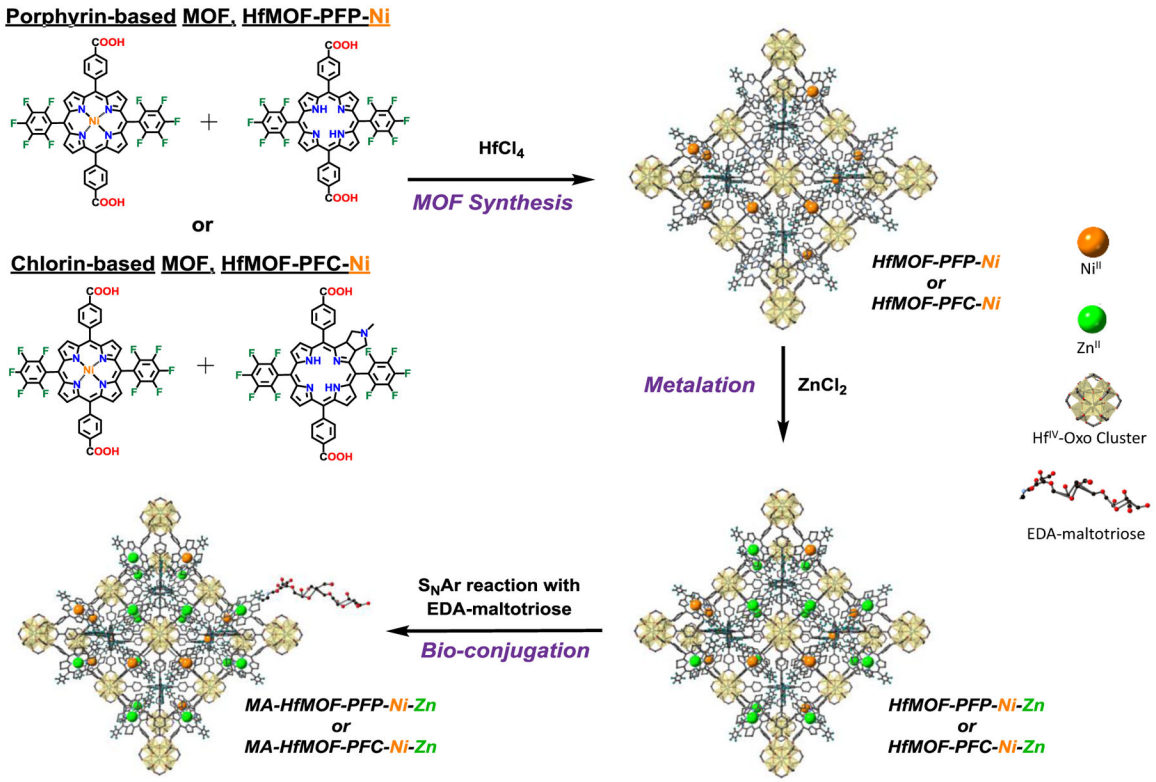

Figure 2:
Synthesis of HfMOF-PFP-Ni-Zn and HfMOF-PFC-Ni-Zn.

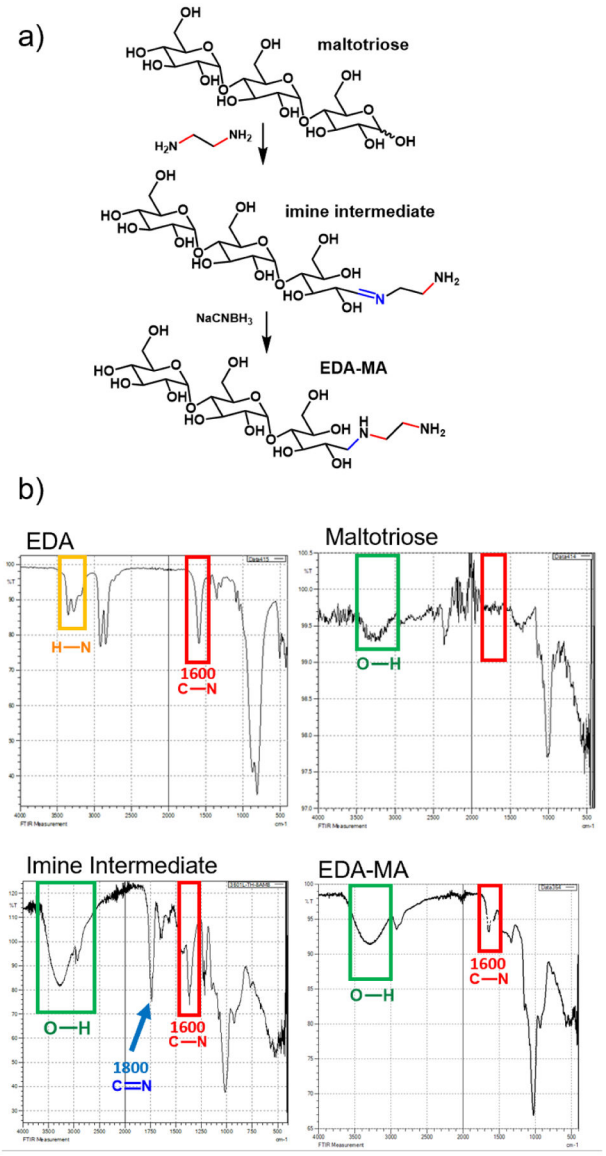

Figure 3.

a) Reductive amination of MA with EDA to yield MA-EDA. The reaction proceeds through an imine intermediate. b**)** Infrared spectroscopy (IR) of reductive amination. *Top left*: IR spectra of EDA and *top right*: maltotiose. *Bottom left*: IR spectra of the reaction mixture showing the imine intermediate and *bottom right:* EDA-MA.

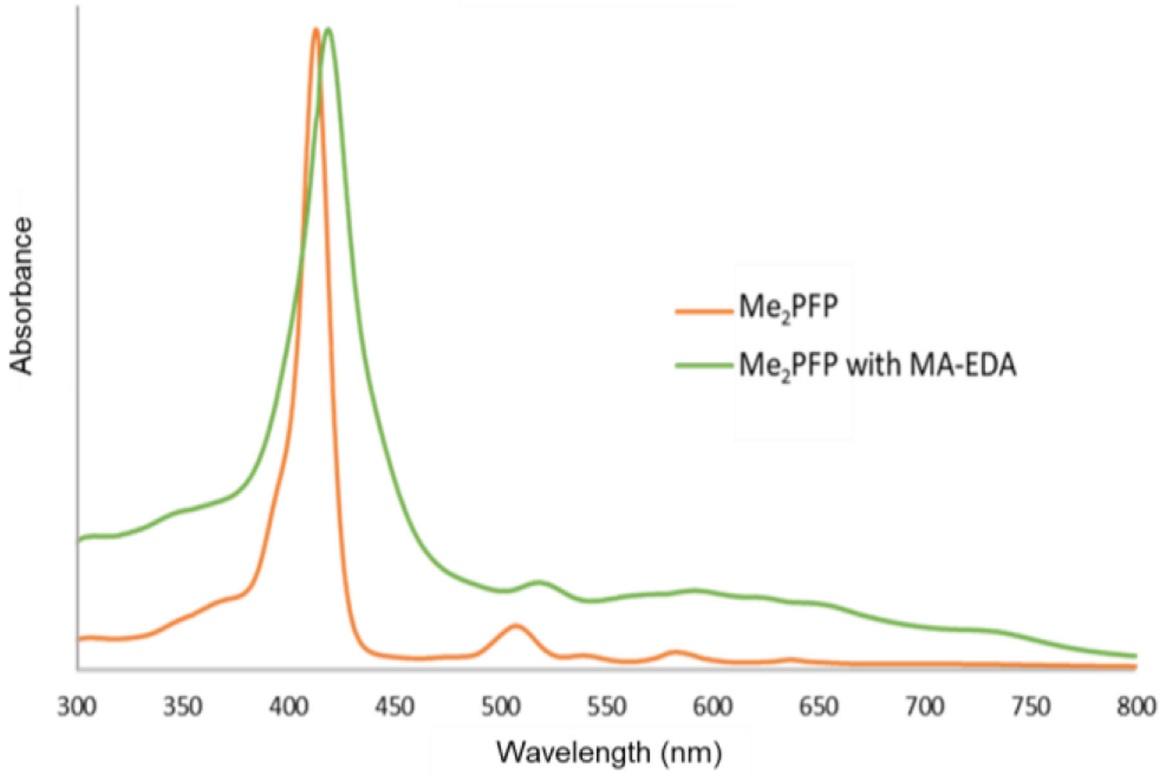

Figure 4.
UV-vis spectra of Me_2PFP dissolved in DMF (orange) and the Me_2PFP after three hours of mixing with EDA and CsF as base.

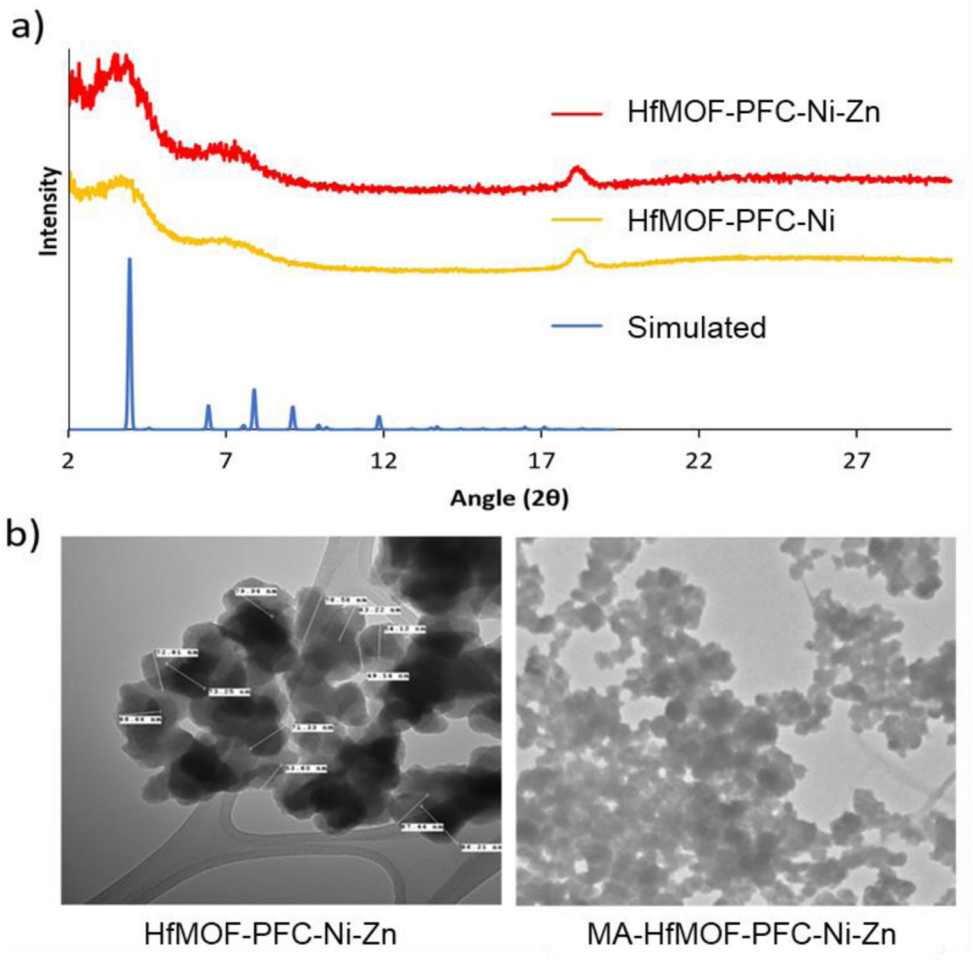

Figure 5.

a) PXRD of HfMOF-PFC-Ni, HfMOF-PFC-Ni-Zn, and the simulated DBP-UiO diffraction pattern.[39,47] b) The TEM images of HfMOF-PFC-Ni-Zn and MA-HfMOF-PFC-Ni-Zn.

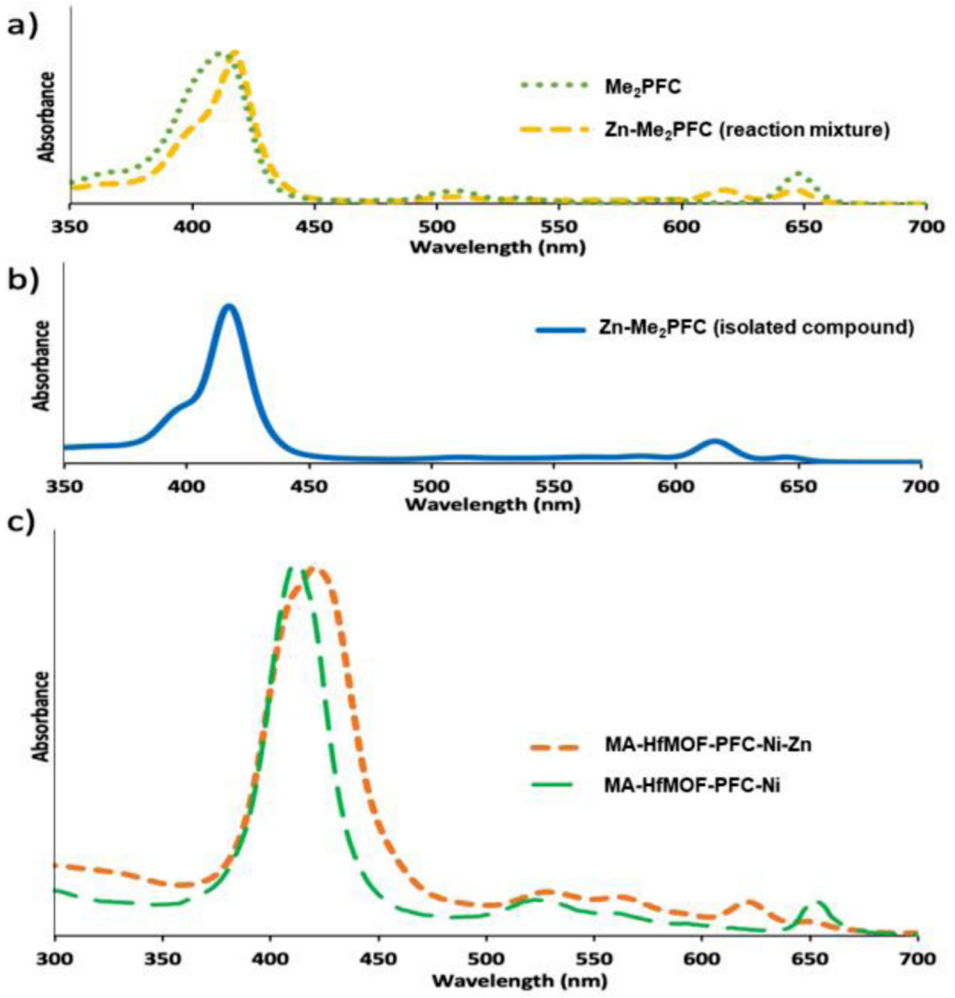

Figure 6.

a) UV-vis spectrum of Me_2PFC before and during metalation with Zn. b) UV-viz of Zn-Me_2PFC. c) UV-vis of HfMOF-PFC-Ni and MA-HfMOF-PFC-Ni-Zn.

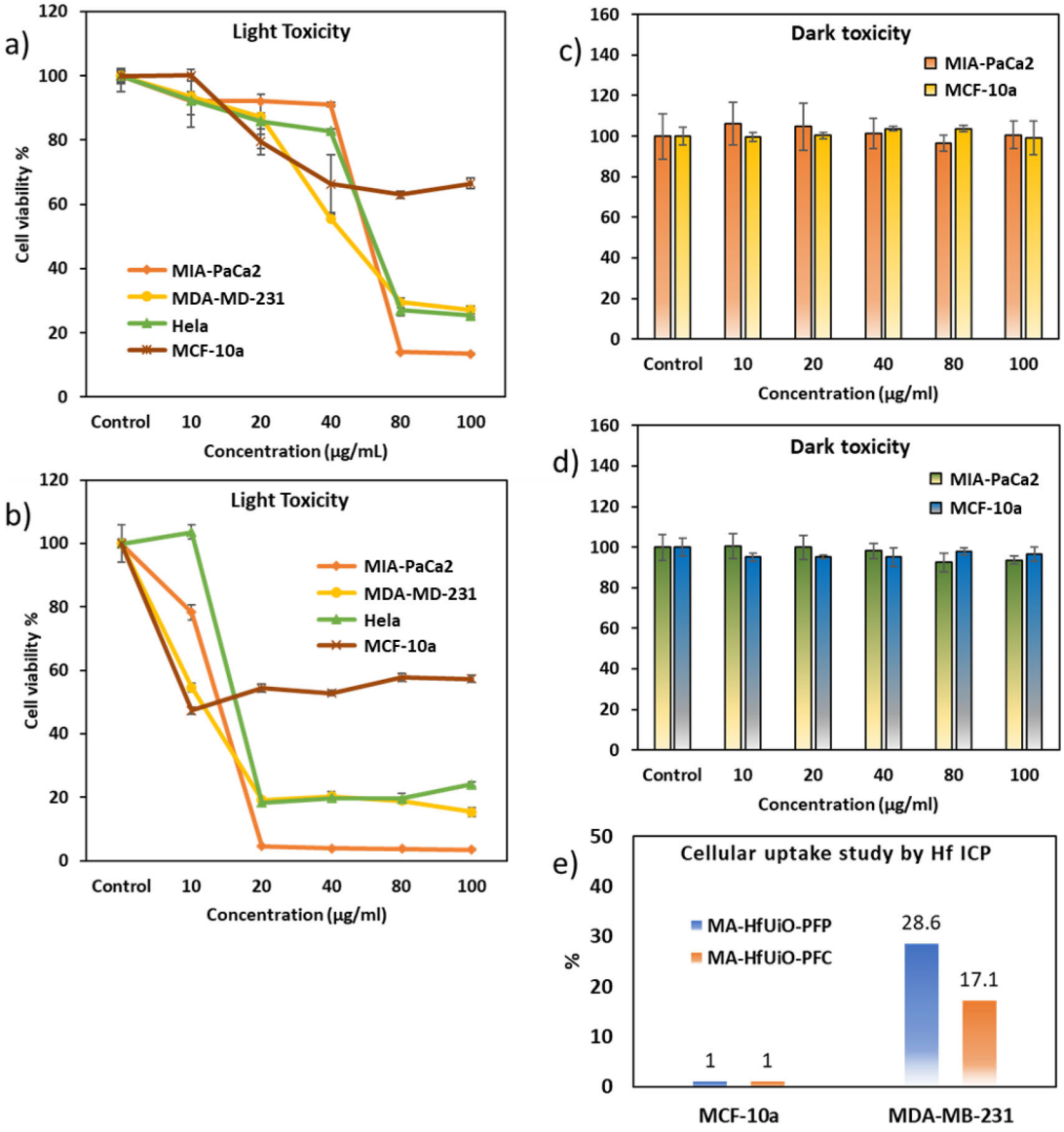

Figure 7.

a) PDT effect of MA-HfMOF-PFP-Ni-Zn on four cell lines, MIA-PaCa2, MDA-MB-231, Hela, and MCF-10a. b) PDT effect of MA-HfMOF-PFC-Ni-Zn on four cell lines, MIA-PaCa2, MDA-MB-231, Hela, and MCF-10a c) Dark toxicity of MA-HfMOF-PFP-Ni-Zn on two cell lines, MIA-PaCa2 and MCF-10a. d) Dark toxicity of MA-HfMOF-PFC-Ni-Zn on two cell lines, MIA-PaCa2 and MCF-10a. e) Cellular uptake study of MA-HfMOF-PFP-Ni-Zn (MA-HfMOF-PFP) and MA-HfMOF-PFC-Ni-Zn (MA-HfMOF-PFC) between MCF-10a and MDA-MB-231.

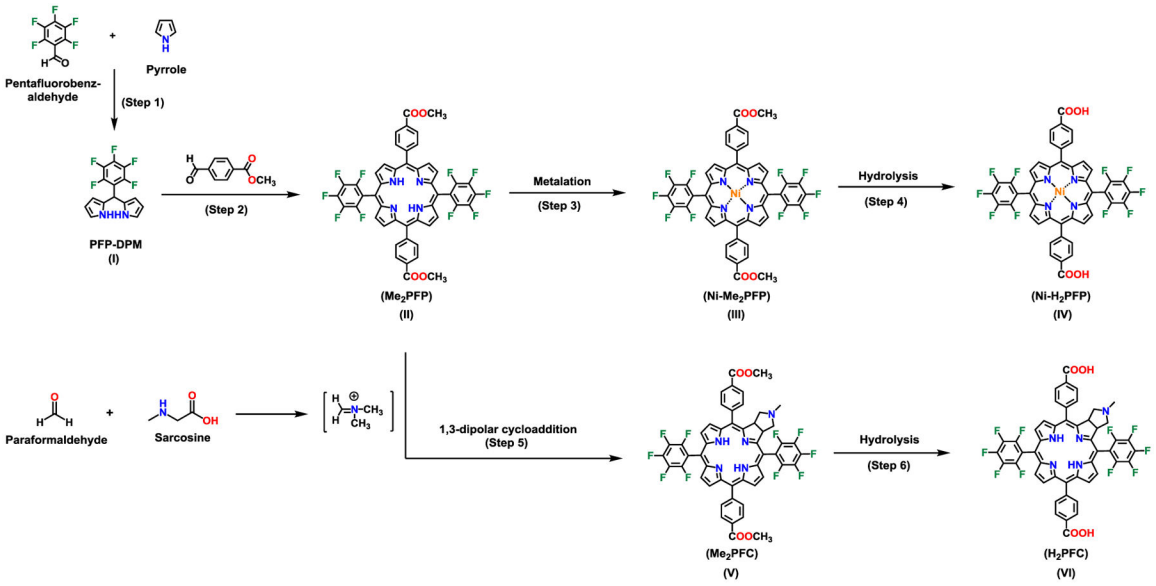

Scheme 1.

Synthesis of 5,15-bis(4-carboxylphenyl)-10,20-bis(pentafluorophenyl)porphyrinato]-Ni(II) (Ni-H_2PFP) and 5,15-bis(4-carboxylphenyl)-10,20-bis(pentafluorophenyl)chlorin (H_2PFC).